Journal of Applied Fluid Mechanics, Vol. 19, No. 1, pp. 3429-3443, 2026. Available online at www.jafmonline.net, ISSN 1735-3572, EISSN 1735-3645. https://doi.org/10.47176/jafm.19.1.3483



Experimental Study on Cavitation Flow Structures of Water-jet Pump

Y. Long^{1†}, C. Tian¹, R. Zhu¹, D. Wang², and J. Chen³

National Research Center of Pumps, Jiangsu University, Zhenjiang, Jiangsu, 212013, China
 School of Mechanical Engineering, Shanghai Jiaotong University, Shanghai, 200240, China
 Marine Design & Research Institute of China, Shanghai, 200011, China

†Corresponding Author Email: longyun@ujs.edu.cn

ABSTRACT

This study presents an experimental investigation into the cavitation flow structures within a water-jet pump, conducted using high-speed photography on a closed-loop test platform. The study captures the temporal evolution of cavitation structures and identifies five typical types: Sheet Cavitation, Cloud Cavitation, Tip Clearance Cavitation, Tip Vortex Cavitation, and Perpendicular Cavitation Vortex (PCV). The evolution of these cavitation structures under varying Net Positive Suction Head available (NPSHa) conditions is analyzed in detail. Based on a combined analysis of cavitation performance curves and flow visualizations, the study reveals that increased cavitation causes the expansion and interaction of PCVs, which block blade passages and result in significant flow separation, ultimately leading to substantial reductions in head and efficiency. Furthermore, the study establishes a quantitative correlation between cavitation vortex structures and pump performance, thereby providing a scientific basis for predicting cavitation-induced degradation. Based on binarized high-speed photography images, the study quantitatively measures vapor volume fractions at various cavitation stages, revealing the relationship between cavitation region expansion and pump performance degradation. It thereby provides visual evidence of cavitation development. This work offers valuable insights into the mechanisms of cavitation evolution and provides engineering guidance for improving the performance of water-jet pumps.

Article History

Received March 20, 2025 Revised June 18, 2025 Accepted August 8, 2025 Available online November 5, 2025

Keywords:

Water-jet pump High-speed photography Cavitation Cavitation flow structure

1. Introduction

Cavitation is a phenomenon of cavitation of vapors or gases inside a liquid or at a liquid-solid interface due to low pressure in a liquid (Pearsall, 1974), which can be studied experimentally and numerically (Dehghan et al., 2024). Preventing cavitation, which can seriously damage fluid machinery, is a key focus for hydraulic machinery designers. High-speed photography experiments are a common means of studying cavitation (Pearsall, 1957). Laberteaux et al. (1998) used high-speed photography to observe the fluid structure within a confined region of attached cavitation. Cavitation flow is characterized by a complex unsteady two-phase turbulence featuring mass, momentum, and energy exchange between the bubbles and the fluid. Therefore, it is essential to study cavitation flow in jet pumps and formulate effective strategies for cavitation mitigation. Accurate prediction and simulation of cavitation vortices remain a significant challenge to computational fluid dynamics (CFD) techniques. In recent years, with advances in CFD, numerical simulation of cavitation flow based on appropriate cavitation models has attracted growing interest (Liu et al., 2011; Shao et al., 2010; Westra et al., 2010; Wu et al., 2011; Zhang et al., 2019). Tong et al. (2023) proposed an early cavitation diagnosis method combining vibration signal neural networks and high-speed photography to improve energy efficiency and mechanical reliability of centrifugal water pumps moved closer to "centrifugal water pumps. Recent work by Dehghan et al. (2024) has highlighted the importance of evaluating measurement uncertainties in experimental cavitation studies, particularly in the assessment of head and efficiency. Quantitative uncertainty estimation not only improves the credibility of experimental findings but also ensures reproducibility across different testing systems. This approach provides a methodological reference framework for the present study.

The water jet propulsion pump plays a critical role in marine propulsion systems, requiring high efficiency and

Nomenclature					
Q	volumetric flow rate	v_I , w_I	absolute / relative velocity		
Н	pump head, defined as the energy increase per unit weight of liquid	$h_{c ext{-}k}$	hydraulic loss between points c and k		
H	hydraulic efficiency	$NPSH_a$	Net Positive Suction Head available		
N	shaft power input to the pump	$NPSH_r$	Net Positive Suction Head required		
N	rotational speed of the impeller	TLV	Tip Leakage Vortex		
Dj	impeller inlet diameter	TLVC	Tip Leakage Vortex Cavitation		
P_s, P_d	static pressure at impeller inlet /guide vane outlet	SC	Sheet Cavitation		
v_s , v_d	flow velocity at impeller inlet /guide vane outlet	CC	Cloud Cavitation		
z_s , z_d	elevation at impeller inlet/guide vane outlet	CCV	Cloud Cavitation Vortex		
p_{v}	saturated vapor pressure of the fluid	PCV	Perpendicular Cavitation Vortex		
p_c, p_k	surface pressure /local pressure near leading edge	TSV	Tip Separation Vortex		

strong anti-cavitation capabilities. The water jet pump's design primarily emphasizes achieving high-speed output via impeller and diffuser optimization while catering to specific operational requirements such as cavitation resistance, low noise, and minimal vibration. Cavitation in water jet pumps causes a rapid decrease in efficiency and an increase in noise levels. Prolonged cavitation results in progressive damage to hydraulic components. The erosion of hydraulic surfaces reduces the efficiency of energy transfer and results in costly maintenance (Li et al., 2019). In light of the aforementioned factors, it is imperative to improve the cavitation resistance of pumps.

Extensive research has been conducted on the development of cavitation. Willard (1953) utilized a pulsed ultrasonic generator to produce high-intensity ultrasonic pulses in the water. The formation and evolution of bubbles were recorded by employing a highspeed camera. Four stages of cavitation in water were identified: an initial stage in which microscopic bubbles emerged in the water; a development stage where the bubbles expanded and contracted intermittently in reaction to shifts in ultrasonic pressure; a rupture stage where the bubbles burst rapidly once they reached a critical radius, releasing high-temperature, high-pressure gases; and a subsequent stage during which the rupture of the bubbles created secondary bubbles and shock waves. Zhao et al. (2022) analyzed the hydrodynamic load variations of the impeller using time-frequency analysis under various cavitation states. In addition, the evolution of the tip leakage vortex (TLV) in the near and far fields was further examined under the influence of cavitation. It was discovered that cavitation promotes TLV formation and enhances its downstream intensity. Cavitation bubbles further expedite the instability of the TLV, leading to earlier breakdown and interaction with the shedding vortices formed by adjacent vortex lines and cavitation on the blade surface. Long et al. (2021) employed high-speed photography to capture the cavitation flow structure in a water jet pump to reveal the dynamics of cavitation evolution. The interaction between cavitation and vortex was further investigated via numerical simulations. The research exposed the flow characteristics in high-velocity regions under varying cavitation stages. The isosurface vortex structure analysis summarizes the primary factors that impact the

development of vortex structures in high-velocity regions.

In our previous studies (Long et al., 2021). On the cavitation flow structures in water-jet propulsion pumps under various operating conditions, we characterized multiple cavitation forms and detailed the formation, development, and dissipation processes of cavitation vortices, as shown in Fig 1. Building on these findings, the present study focuses on a mixed-flow water-jet propulsion pump with a shrinkage guide vane, aiming to elucidate the evolution mechanism of cavitation flow structures and their impact on pump performance.

This paper investigates a water jet propulsion pump, specifically, a mixed-flow pump equipped with a shrinkage guide vane, designed to reduce hull space while maintaining high energy density. The experimental study aimed to elucidate the evolution mechanism of cavitation flow structures in the water jet propulsion pump. High-speed photography was employed on a comprehensive performance test platform, we obtained the characteristics of the cavitation vortex during the onset and development of cavitation. This allowed us to analyze the evolution patterns of cavitation flow structures.

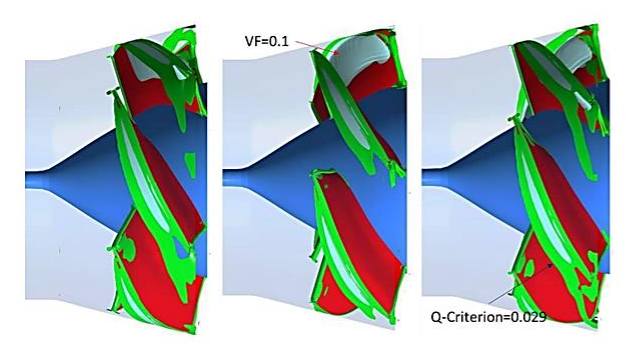
2. CAVITATION TEST

2.1 Pump Cavitation Basic Equations

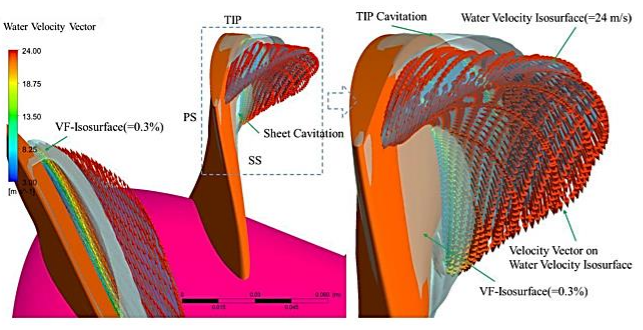
According to the principle of cavitation based on saturated vapor pressure, when fluid pressure drops to its saturated vapor pressure (p_v), water transforms into vapor bubbles. This transformation is described by Eq. (1), which outlines the fundamental equation for pump cavitation analysis (Pan & Yuan, 2013).

$$\left[\left(z_c + \frac{p_c}{\rho g} + \frac{v_c^2}{2g} \right) - z_K - h_{c-K} - \frac{p_V}{\rho g} \right]
+ \left(\frac{p_V}{\rho g} - \frac{p_K}{\rho g} \right) = K_1 \frac{v_1^2}{2g} + K_2 \frac{w_1^2}{2g}$$
(1)

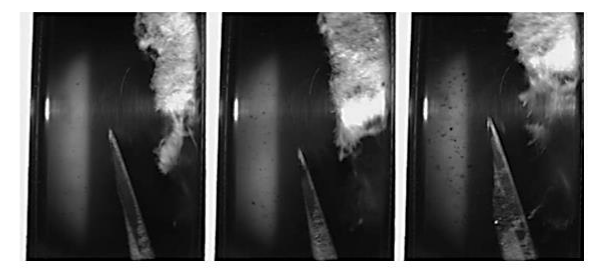
In this equation, p_v is the fluid's saturated vapor pressure, p_k denotes the pressure at point K near the leading edge, and p_c is the suction fluid surface pressure.



The cavitation flow structure and its evolution law at different times in the critical cavitation condition



Isosurface set on the impeller blade



Cavitation vortex structure under critical cavitation conditions at different flow rates

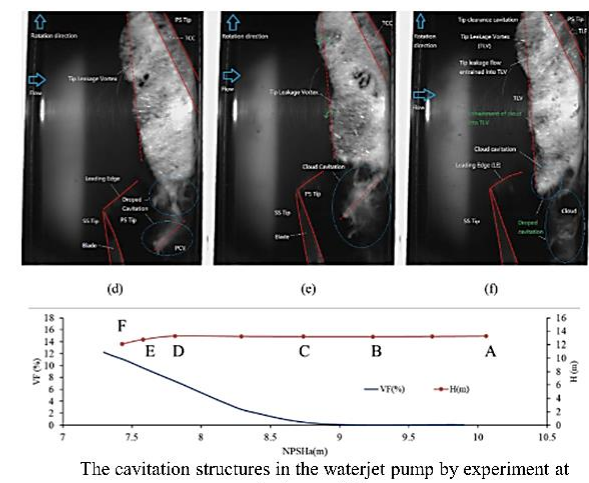


Fig. 1 Cavitation analysis of pumps under different conditions (Long et al., 2021)

Other terms include v_c , the suction fluid surface velocity (m/s), z_c , the height of the fluid surface, z_k , the height at point K, h_{c-k} , representing hydraulic loss from point c to k, v_l , the absolute velocity, and w_l , the relative velocity, both in meters per second.

The Available Net Positive Suction Head $(NPSH_a)$ represents the available energy of the liquid at the pump inlet, relative to the energy required to overcome vapor pressure. This value, is typically computed based on the hydraulic parameters, is derived from the terms on the left side of the square brackets. The same formula for NPSH_a is given in Eq. (2):

$$NPSH_a = \left(z_c + \frac{p_c}{\rho g} + \frac{v_c^2}{2g}\right) - z_K - h_{c-K} - \frac{p_V}{\rho g}$$
 (2)

In contrast, the Required Net Positive Suction Head $(NPSH_r)$, determined by the pump's internal flow, addresses terms on the right side:

$$NPSH_r = K_1 \frac{v_1^2}{2g} + K_2 \frac{w_1^2}{2g} \tag{3}$$

By combining Eqs. (1), (2), and (3), we obtain the physical expression for cavitation conditions in the pump, recognized as the foundational equation for pump cavitation:

$$NPSH_a + \left(\frac{p_V}{\rho g} - \frac{p_K}{\rho g}\right) = NPSH_r$$
 (4)

The term 'Head' (H), defined as the energy increase per unit weight of liquid from the pump inlet (point 2 D_i before the impeller flange) to the outlet (point 2 D_d after the guide vane outlet), is measured in meters. This relationship is provided in Eq. (5):

$$H = \frac{p_{\rm d} - p_{\rm s}}{\rho g} + \frac{v_{\rm d}^2 - v_{\rm s}^2}{2g} + z_{\rm d} - z_{\rm s} \tag{5}$$

where ps is the static pressure of 2Dj in front of the impeller inlet flange, in Pa; pd is the static pressure of 2Dd behind the guide vane outlet flange, in Pa; vs is the velocity of 2Dj in front of the impeller inlet flange, in m/ s; vd is the velocity of 2Dd behind the guide vane outletflange, in m/s; zs is the distance from the reference surface 2Dj in front of the impeller inlet flange, in m; zd is the 2Dd position behind the guide vane outlet flange to the reference plane Distance in m.

2.2 High-Speed Photographic Acquisition System and Pump Comprehensive Performance Test Loop

As shown in Fig. 2, the experimental test loop and the high-speed imaging system are schematically illustrated. The detailed parameters of both the test loop and the highspeed imaging system are provided in Fig. 2, while the design parameters of the pump and the imaging system are listed in Table 1.

The flow rate in this study was measured using a calibrated electromagnetic flow meter installed upstream of the pump, ensuring high accuracy and stability under various operating conditions. The differential head was determined by recording the static pressure at the suction and discharge flanges of the pump using high-precision pressure transducers. According to standard practice in cavitation performance evaluation, the onset of cavitation

Table 1 Technical Specifications of the Water-Jet Pump
Test Rig

Parameter	Unit	Value
Flow rate, Q	m³/s	0.46
Head, H	m	13
Rotational speed, n	r/min	1450
Impeller inlet diameter, D_j	mm	270
Impeller outlet diameter, D_d	mm	250
Tip clearance	mm	1
Impeller blade inlet hub	mm	120
diameter, D_{hlE}		
Guide vane outlet rim	mm	260
diameter		
Shaft power, N	kW	70
Specific speed, n_s	-	524.3
System accuracy	%	0.2
Max frame rate	Fps	4467
Resolution	pixels	1008×1008
Camera-to-glass distance	m	0.5
Image interval per rotation	0	2

is typically defined as the point at which the total dynamic head drops by 3% from its non-cavitating baseline value. This criterion provides a quantitative basis for identifying incipient cavitation and is widely adopted in both academic and industrial studies (Dehghan & Shojaeefard, 2022).

3. RESULT ANALYSIS

3.1 Cavitation Performance Curves and Cavitation Structures

Prior to conducting the analysis, it is important to define and categorize the typical cavitation types observed in jet pumps, based on relevant literature and monographs, as illustrated in Fig 2.

(1) Sheet cavitation typically occurs near the blade's leading edge and manifests as a thin vapor layer adhered to the blade surface (Franc & Michel, 2006). Its location is closely related to the angle of attack: it tends to form on the suction side under positive incidence angles and on the pressure side under negative incidence angles.

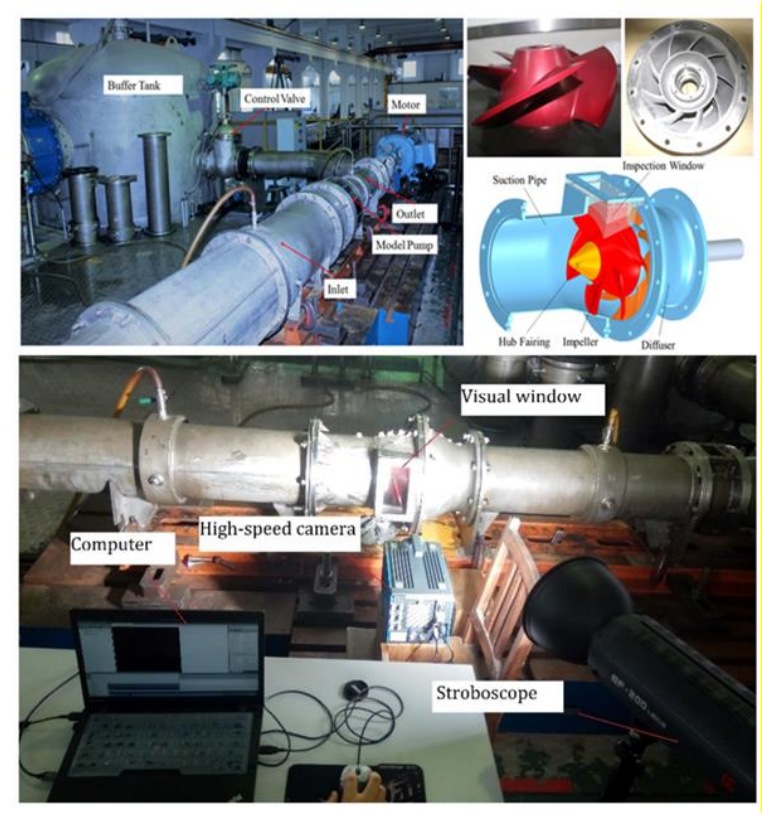


Fig. 2 High-speed photographic acquisition system and Pump Comprehensive Performance Test Loop

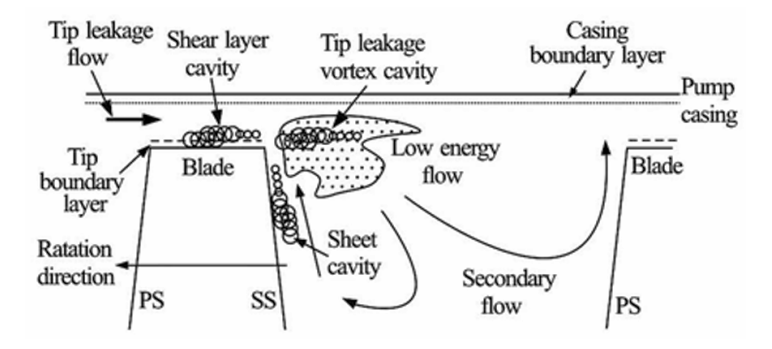


Fig. 3 Flow structures around vane tip clearance in an axial pump (Luo et al., 2016)

- (2) Cloud cavitation typically results from the breakup of developed sheet cavitation and manifests as unsteady, cloud-like or misty structures. The cavity interface is characterized by fluctuations and turbulence, exhibiting strong instability. This leads to significant oscillations in cavitation length (Franc & Michel, 2006).
- (3) Tip Clearance Cavitation: This form of cavitation typically occurs and remains within the blade tip clearance. It is caused by the high-speed leakage flow between the pressure and suction sides of the blade due to blade rotation, leading to the formation of a tip separation vortex (TSV).
- (4) Tip Leakage Vortex Cavitation: The high-speed tip clearance flow interacts with the main flow along the suction surface, forming a tip leakage vortex. The low-pressure core of the vortex induces cavitation within the tip clearance vortex (Rains, 1954). Additionally, this vortex may entrain vapor bubbles from sheet cavitation on the suction side into the high-speed jet within the tip clearance, further enhancing cavitation in the blade tip region.

3.2 Cavitation Structures and the Evolution at Non-Cavitation Condition

During high-speed imaging, images were captured for every 2° rotation of the impeller, and 180 images are taken in one rotation of the impeller. In general, transient cavitation analysis focuses on flow structures within the rotation of a single blade. The impeller used in this study has five blades, so the rotating angle of a single blade is 72°. Six images are equally spaced to show the cavitation flow structures, corresponding to a 12° interval between successive images.

Figure 4 depicts the cavitation flow structures and associated flow field features at specific time steps under the Non-Cavitation Condition corresponding to Point A. Results indicate that although the performance curve of the pump exhibits no significant deviation during this stage, tip vortex cavitation is observed in the blade tip region. This occurs because the vortex core pressure of the Tip Leakage Vortex remains low, leading to cavitation in the vortex core region. Influenced by the vortex produced by the tip separation, Tip Clearance Cavitation develops occurs in the tip clearance of the blade. Simultaneously, a vortex filament forms near the blade's tip. The Tip Leakage Vortex Strip rotates counter to the impeller's rotation. When the impeller rotates 12°, the Tip Leakage Vortex Cavitation starts to detach and migrate toward to the adjacent blade. The bubbles separate from the blade and are entrained into the main flow. Between the linear boundary of Tip Leakage Vortex Cavitation and the suction surface of the blade, numerous vortex filaments are observed in the frontal section of the blade. At a rotation angle of 24°, the vortex cavitation collapses in the rear section of the blade, and at 36° rotation, the TLVC progressively collapses toward the middle region of the blade channel. At 48 and 60 degrees, no cavitation bubbles are observed on the blade's pressure surface, and the TLVC exerts minimal influence on the adjacent blade's pressure surface. Consequently, the pump's performance curve remains largely unaffected under these conditions.

3.3 Cavitation Structures and the Evolution at Cavitation inception condition

Figure 5 shows the cavitation flow structures and the evolution of the water-jet pump at the Cavitation inception condition Point B. It can be seen that at the onset of cavitation, there is a prominent Tip Vortex Cavitation (TVC) in the tip region. Compared with the cavitation state of point A, the cavitation at point B is considerably more intense. This is primarily attributed to the low pressure at the vortex core of the Tip Leakage Vortex (TLV). As the vacuum pump continues to operate, the pressure in the entire system environment is decreasing. The pressure in the vortex region is reduced, further promoting bubble formation in the vortex core. Consequently, the Sheet Cavitation (SC) develops along the suction surface near the leading edge of the blade, and the TLV causes the Sheet Cavitation to be entrained into the Tip Leakage Vortex strip. A triangular cloud cavitation structure has developed in the region between the suction surface and the Tip Leakage Vortex boundary. The Tip Clearance Cavitation is generated at the tip clearance, and a vortex structure is also observed at the suction surface near the tip of the blade. The TLV strip extends linearly and rotates counter to in the direction opposite to the impeller rotation. From Fig. 5, the cloud cavitation of the last adjacent blade can be observed. The vortex cavitation perpendicular to the blade is observed near the pressure surface of the blade, referred to as the Perpendicular Cavitation Vortex. The PCVs occur in isolated regions on the blade surface, thus exerting minimal influence on pump performance. As the pressure is reduced and cavitation gradually covers the suction surface of the blade, the interaction begins to occur between cavitation zones of adjacent blades. The Perpendicular Cavitation Vortex extends from the suction surface of the initial blade to the pressure surface of the adjacent blade. When the Perpendicular Cavitation Vortex extends between the blades, Cavitation breakdown condition is triggered, causing blockage in the upper region of the blade passage (Tan et al., 2015). This large-scale cloud cavitation vortex structure leads to a rapid decline in pump performance. At the same time, it induces mutual interference between adjacent blades within adjacent blades, resulting in flow separation, particularly along the pressure surface and resulting in the flow instability in the pump (Shi, 2016).

After the impeller rotates 12°, under the entrainment effect of the TLV, the Cloud Cavitation Vortex (CCV) near the tip triangle's trailing edge is initially formed. The Cloud Cavitation Vortex is mainly affected by Sheet Cavitation, the main flow, and the Tip Leakage Flow. It begins to detach at the trailing edge of the triangle. The direction of rotation is gradually shifting from being counter to impeller rotation to aligning perpendicular to the adjacent blades. When the impeller rotates 24°, at the rear

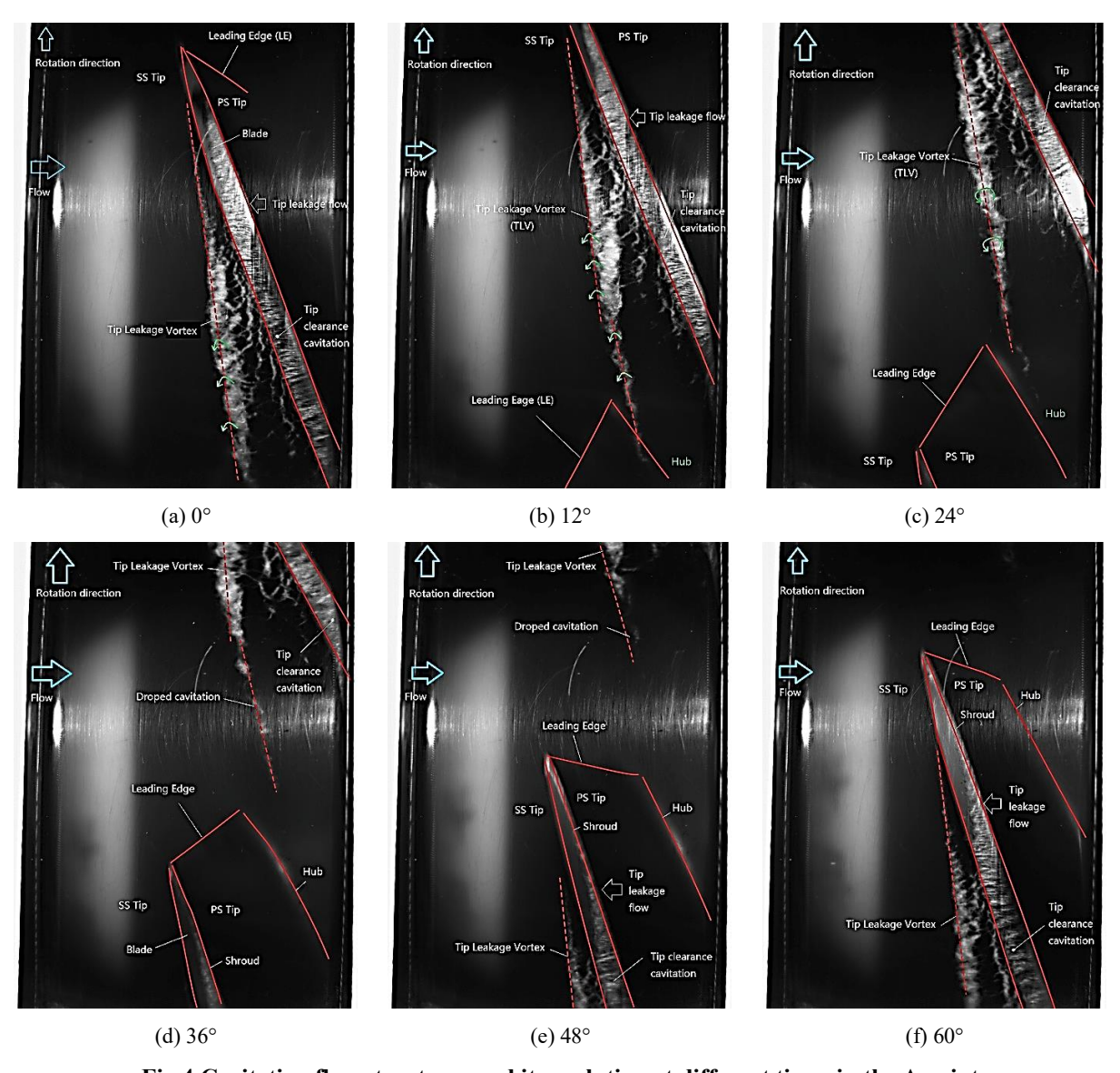
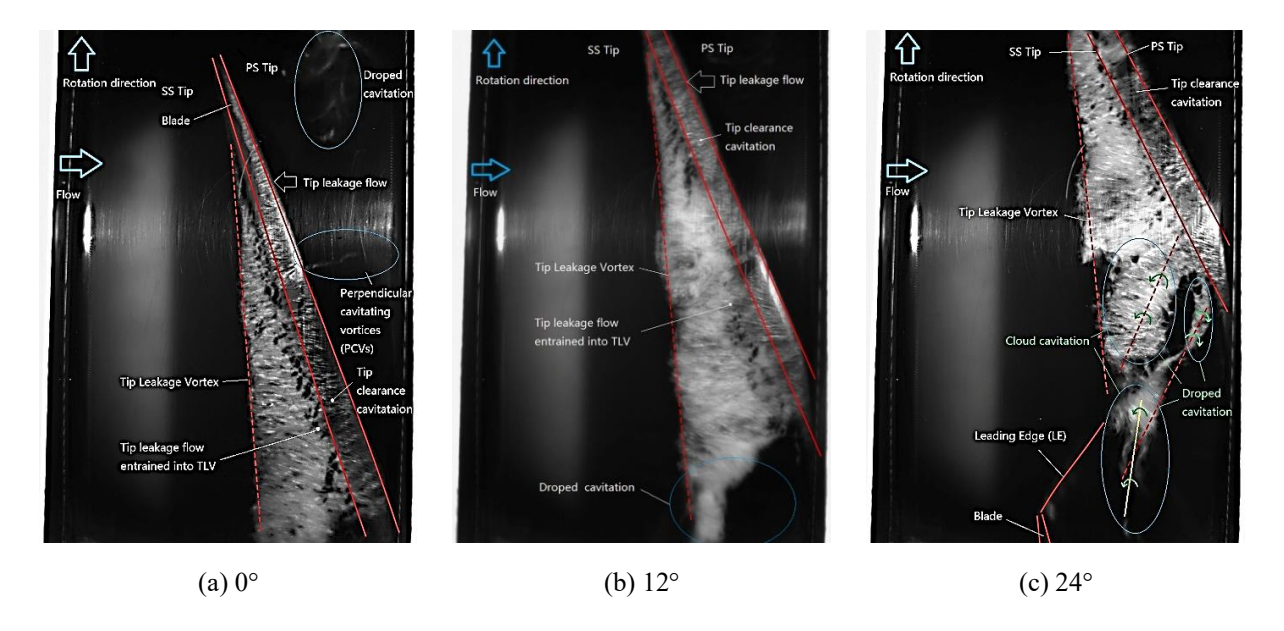


Fig 4 Cavitation flow structures and its evolution at different times in the A point



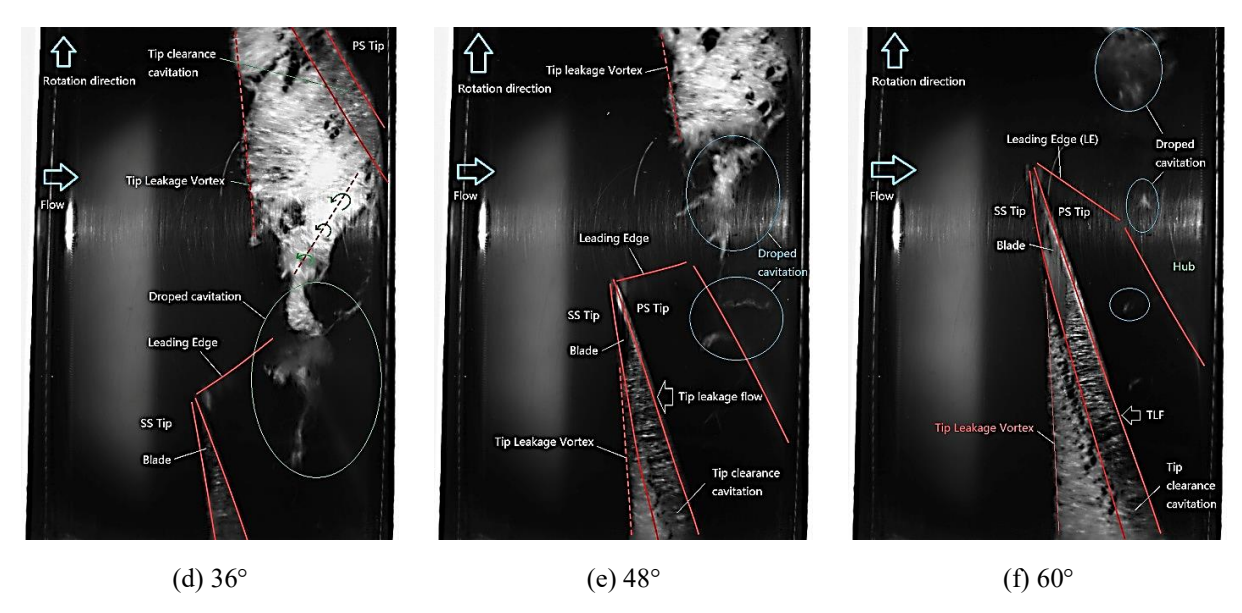


Fig. 5 Cavitation flow structures and its evolution at different times at the B point

edge of the tip cavitation triangle, the detachment the cloud cavitation at the beginning of the last moment can be found, and the significant shedding boundary becomes distinct occurs at this moment, with vortex rotation extending from the suction side of the blade toward the leading edge of the adjacent blade. Downstream of the large-scale cloud cavitation, cavitation vortices with opposite rotation directions are observed adjacent to the suction surface. The cavitation vortex is primarily induced by the tip flow, the main flow, and shedding cloud cavitation. Downstream of the aforementioned vortex structures, the cloud cavitation has fully detached and advected toward the adjacent blade. The rotation direction of the cavitation vortex is consistent with the upstream large-scale cloud cavitation, but the cavitation vortex structure and the upstream reverse cavitation vortex exhibit structural continuity. When the impeller rotates 36°, the cloud cavitation tail begins to break up into numerous discrete bubbles. The detached cavitation moves towards the adjacent blade. Some portions migrate toward the blade pressure surface, while others move toward the tip clearance. The bubbles move toward the pressure surface of the blade, which leads to the blockage of the blade passage and causes flow separation near the pressure surface. When the impeller rotates 48°, the cavitation bubbles undergo rapid collapse during advection during the movement. The detached cavitation vortex continuously oscillates, and the oscillating vortex lacks a stable low-pressure core. The reverse pressure gradient induces rupture of the vortex structure, leading to its dissipation. Bubbles migrating toward the tip clearance are entrained by the Tip Leakage Flow of the adjacent blade. These bubbles initially move perpendicular to the pressure surface and are gradually deflected toward the pressure surface of the adjacent blade. Subsequently, the Perpendicular Cavitation Vortex (PCV) is subjected to shear and fragmentation by the blade geometry, with a

portion entering the tip clearance and the remainder collapsing near the blade tip's pressure surface.

Given its formation near the blade tip shear layer and its nsteady rupture behavior and absence of a stable vortex core, the PCV is most plausibly attributed to Kelvin–Helmholtz instability, originating from the velocity gradient between the tip leakage flow and the main stream. In contrast, Taylor–Görtler-type vortices, which typically develop under conditions of sustained boundary layer growth over concave surfaces, are less consistent with the transient and spatially localized characteristics observed here.

3.4 Cavitation Flow Structures and the Evolution at Cavitation development transition condition

Figure 6 illustrates the cavitation flow structures and their progression in the water-jet pump under the Cavitation development transition condition at Point C. From Fig. 6, it is evident that a prominent Tip Vortex Cavitation has developed in the tip area. Compared to the cavitation observed at Point B, the cavitation intensity at Point C is significantly higher. This is particularly evidenced by denser cavitation in the triangular tip region and larger-scale cavities extending from its trailing edge.

At the initial stage of rotation, cloud cavitation is observed forming on the pressure surface of the adjacent blade. A Perpendicular Cavitation Vortex (PCV) appears near the blade's pressure surface and begins interacting with the tip clearance flow. As detailed earlier, the PCV undergoes shearing and fragmentation induced by blade-surface interactions, with part of it entering the tip clearance and the remainder collapsing near the tip region of the pressure surface. Influenced by the main flow, the PCV is carried downstream in a rolling motion. As shown in Fig. 6(b), at 12° of impeller rotation, the Cloud Cavitation Vortex

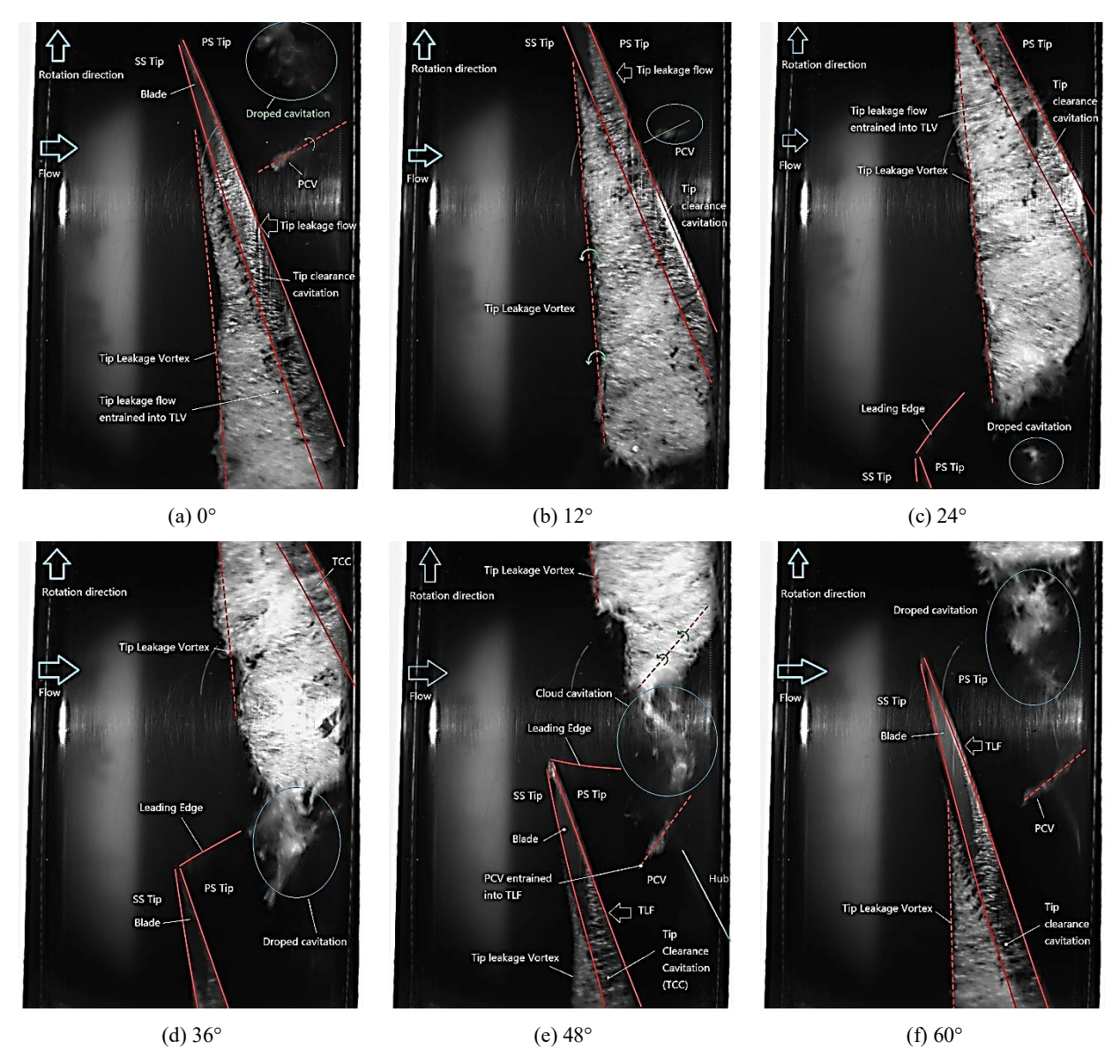


Fig. 6 Cavitation flow structures and its evolution law at different times in the C point

trailing the triangular region begins to detach. By the time the impeller rotates 24°, the vortex rotation direction shifts. The rotation transitions from the suction side of one blade to the leading edge of the adjacent blade, accompanied by the emergence of cloud cavitation. At 36° of rotation, the cloud cavitation tail starts fragmenting into larger bubble clusters. These detached cavitation regions migrate toward the neighboring blade, with some moving to the blade's pressure surface and others toward the tip clearance.

At 48° of impeller rotation, the detached bubble clusters undergo rapid collapse and reduction in volume during their movement, leaving only a few smaller bubbles while the detached cavitation vortex continues to oscillate without stabilizing. The bubbles migrating toward the tip clearance are entrained by the adjacent blade's tip leakage flow. Their direction gradually aligns perpendicular to

perpendicular to the pressure surface, eventually reaching the adjacent blade's pressure surface. Subsequently, the PCV is once again subjected to shear and fragmentation by the blade by the blade, with part of it entering the tip clearance and the remaining portion collapsing at the tip region of the pressure surface.

3.5 Cavitation Flow Structures and the Evolution at the I critical Cavitation Condition

Figure 7 shows the internal cavitation flow structures at the I critical Cavitation Condition (Point D). A significant Tip Vortex Cavitation is formed in the tip region. Cavitation at Point D is markedly more intense than at Point C. Larger scale cavitation bubbles also appear in the entrained tip leakage vortex.

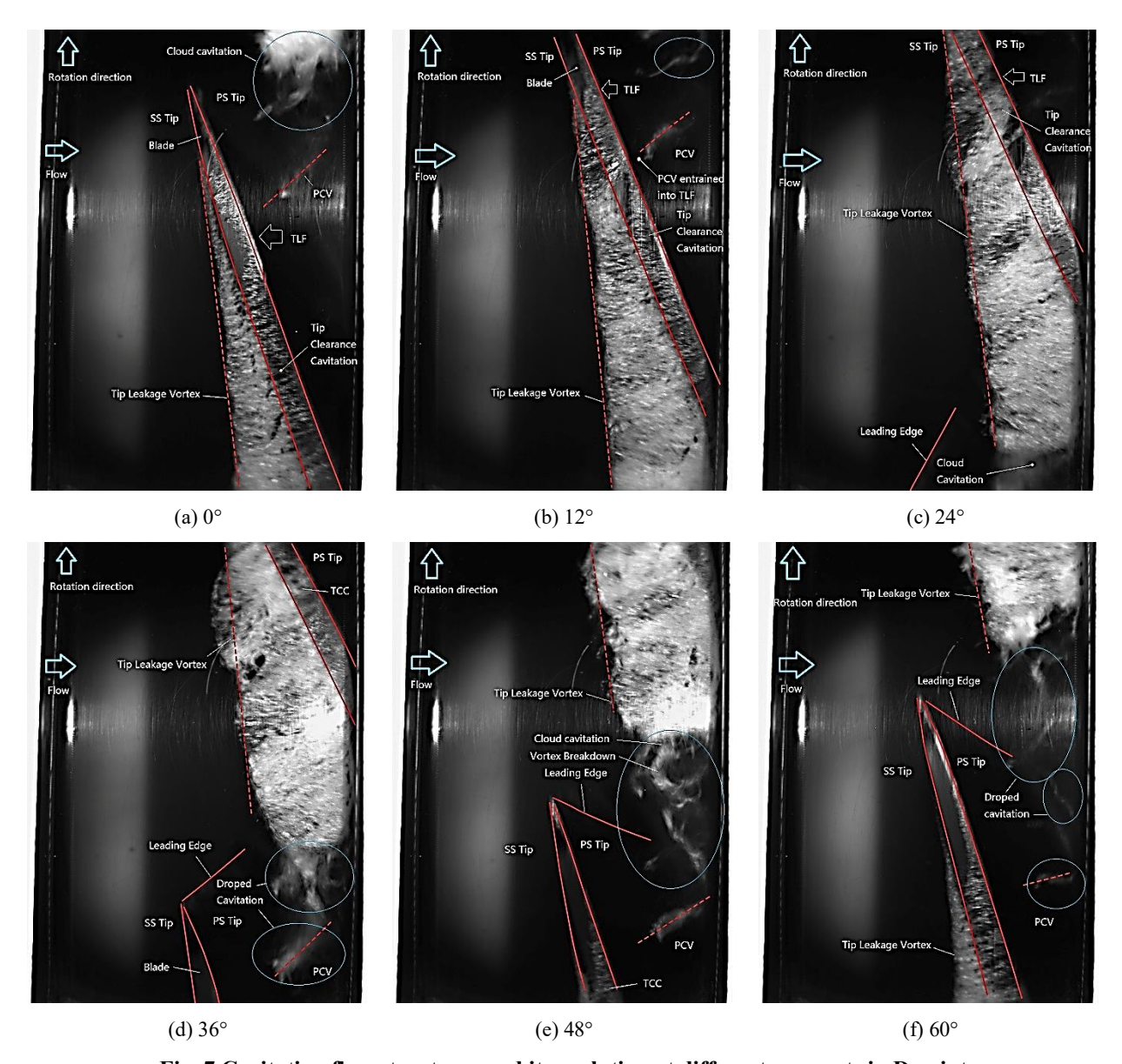


Fig. 7 Cavitation flow structures and its evolution at different moments in D point

Compared to the previous condition, the trailing edge of the triangular region extends towards the main flow direction, and the scale of shedding cavitation at the trailing edge of the triangular region is larger.

At first, Cloud Cavitation is initially observed the Cloud Cavitation from the nearby blade of the pressure surface. This cloud cavitation is denser and broader than that observed at Point C. In addition, due to the mainstream effect, the Perpendicular Cavitation Vortex is advected downstream by the main flow. In Fig. 7(b), it is evident that when the impeller rotates 12°, there is an intense cavitation development, and there is no shedding of cloud cavitation vortex as seen at the previous condition at the trailing of the triangle. When the impeller rotates at 12° and 24°, larger cavitation bubbles are clearly visible within the entrained Tip Leakage Vortex. In addition, cloud cavitation gradually weakens at the trailing edge of the tip triangle of the tip triangle during impeller rotation. When the impeller turns at 36°, the blade pressure surface the PCV becomes visible on the blade pressure surface, which enters the tip clearance flow. The detached

cavitation moves toward the adjacent blade, with a portion moving toward the blade pressure surface and the other portion moving toward the tip clearance. When the cavitation moves toward the pressure surface of the blade, it induces blockage within the flow passage, and leads to flow separation along the pressure surface. As for the cavitation moving toward the tip clearance, it is entrained by the tip leakage flow of the adjacent blade, and its direction initially aligns perpendicular to the pressure surface. When the impeller rotates to 48 degrees, it is observed that the vortex separating from the cloud cavitation undergoes disruption and large bubbles undergo rapid collapse, with only a few small remnants remaining. The detached cavitation vortex exhibits continuous oscillation and is advected toward towards the adjacent pressure surface. This phenomenon persists from 48 to 60 degrees. The blade shears and fractures the PCV during interaction with the main flow. The strength of the Perpendicular Cavitation Vortex (PCV) has increased compared to the previous state, but its rapid collapse results in a noticeable degradation in pump performance.

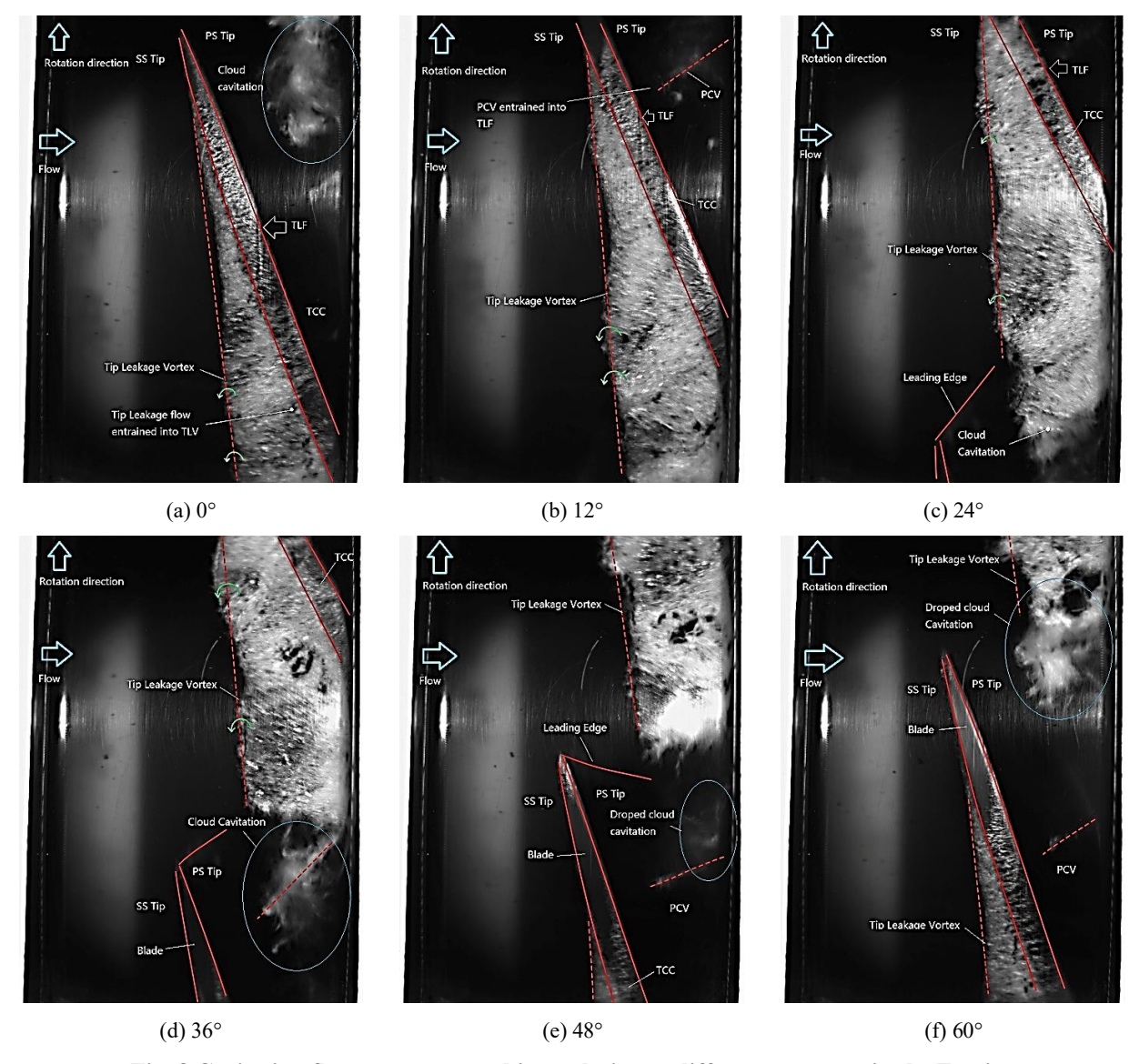


Fig. 8 Cavitation flow structures and its evolution at different moments in the E point

3.6 Cavitation Flow Structure and its Evolution Law at Critical Cavitation Condition

Figure 8 depicts the cavitation flow structures observed at the Critical Cavitation Condition Point E. Fig. 8 highlights the presence of distinct tip cavitation in the blade tip region. In comparison to the cavitation state observed at point D, the cavitation at point E exhibits greater intensity with significantly larger bubble clusters within the entrained Tip Leakage Vortex in the entrained Tip Leakage Vortex. The trailing edge of the triangular region extends to the mainstream. The shedding of cavitation at the trailing edge of the triangle occurs at a larger scale, resulting in more intense entrainment and tumbling.

At the early stage of cavitation development, cloud cavitation is noticeable, originating from the pressure surface of the adjacent blade and extending further into the main flow region beyond point D. When the impeller reaches a rotational angle of 12°, a Perpendicular Cavitation Vortex emerges close to the pressure surface, accompanied by intensified cavitation within the Tip

Leakage Vortex within the Tip Leakage Vortex. As the process progresses, large bubbles are consistently observed at the trailing edge of the triangular tip region. Upon the impeller's rotation to 36°, the cloud cavitation tail undergoes collapse, fragmenting into multiple smaller cavitation zones, which then migrate toward the neighboring blade. This movement begins on the suction side of the blade and proceeds toward the pressure surface of the adjacent blade.

By the time the impeller rotates to 48°, the detached cloud cavitation reorients, aligning perpendicular to the pressure surface due to interactions between the Tip Leakage Flow and the main flow. At 60° of rotation, the cloud cavitation further fragments, causing the main body of the triangular cavitation region to detach and the PCV to be entrained into the tip clearance while rolling with the main flow. At this stage, significant cavitation prevails in the upper region of the flow channel, with detached cavitation clouds occupying a substantial portion of the domain. This severe cavitation disrupts the flow passage, leading to severe flow separation near the blade surface.

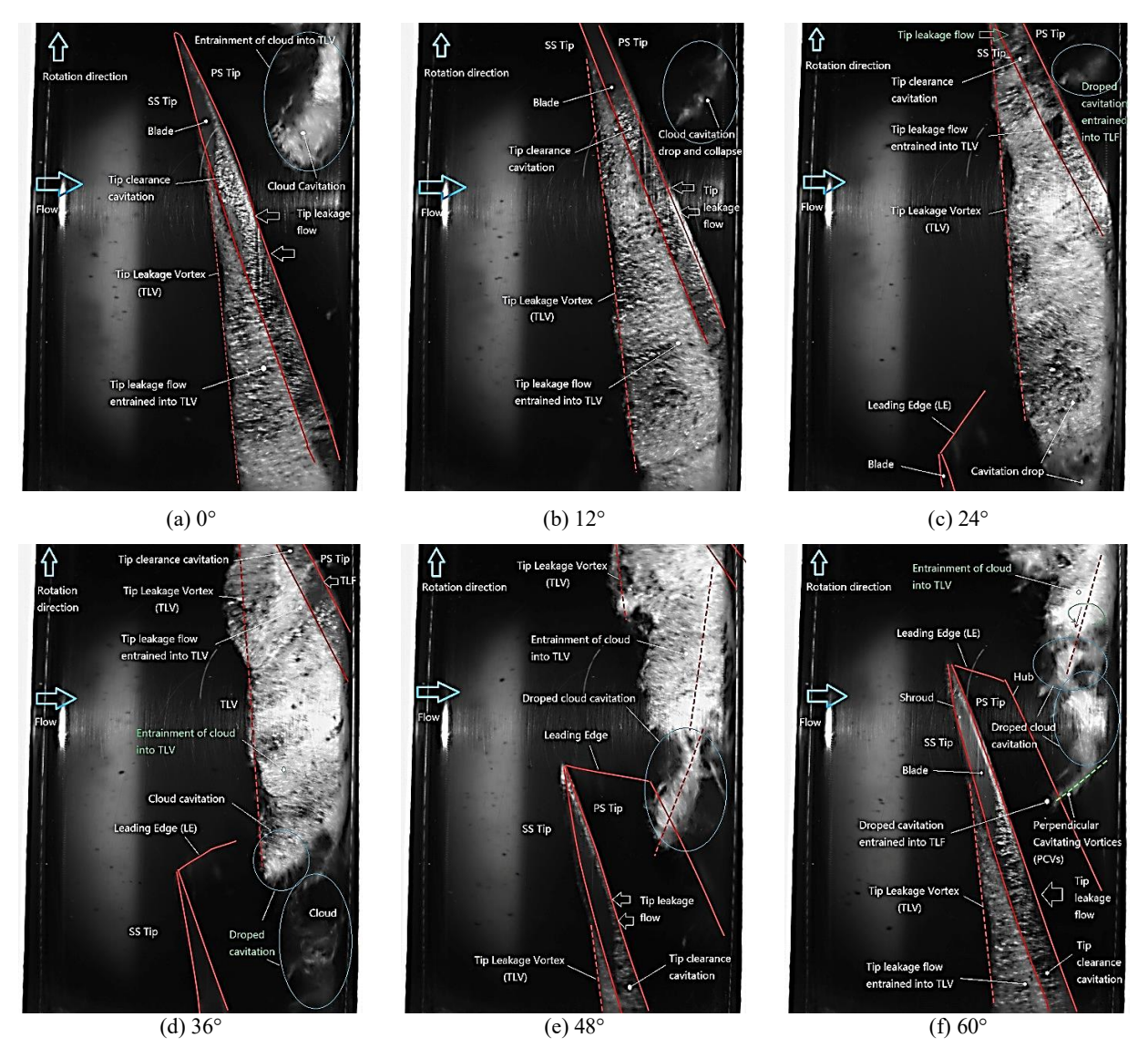


Fig. 9 Cavitation flow structures and its evolution law at different times in F point

Consequently, pump performance is adversely affected, resulting in a 3% reduction in the pump head.

3.7 Cavitation Flow Structures and the Evolution at Cavitation Breakdown Condition

Figure 9 shows the internal cavitation flow structures and the evolution at the Cavitation breakdown condition point F.

As shown in Fig. 9, a severe tip cavitation has developed in the tip region. Compared to Point E, cavitation at Point F is more severe. In addition, there are still more large bubbles in the Tip Leakage Vortex, the cavitation at the trailing of the triangle extends further into the main flow direction, and it is close to the adjacent blade pressure surface. The trailing edge cavitation impinges upon and collapses near the pressure surface before migrating into the tip clearance of the neighboring blade. This process accelerates and facilitates the initiation and progression of cavitation within the adjacent blade region. At the initial stage, cloud cavitation emerges from the pressure surface of a neighboring blade. This cavitation cloud gradually expands across the central flow

region toward the pressure surface of the blade. When the impeller reaches a rotation of 12°, a Perpendicular Cavitation Vortex forms near the blade's pressure surface, triggered by the collapse of the cloud cavitation. This vortex develops as a result of the entrainment caused by Tip Leakage Flow (TLF) and the turbulence generated by the main flow within the blade passage, resulting in detached cloud cavitation oriented perpendicular to the pressure surface. Within the Tip Leakage Vortex, large-scale bubbles are observed undergoing intense rolling motion, with these bubbles subsequently trailing the tip triangle.

At a 24° rotation of the impeller, large detached bubbles migrate toward the blade's pressure surface and enter the tip clearance, forming a more concentrated cavitation layer. Simultaneously, at the trailing edge of the tip cavitation triangle, rolling bubble clusters within the cloud cavitation begin to detach. When the impeller rotates to 36°, the cavitation covering the tip clearance becomes part of the Tip Leakage Cavitation Vortex, and merges with the existing leakage vortex. Detached cloud cavitation is also observed forming at the rear of the

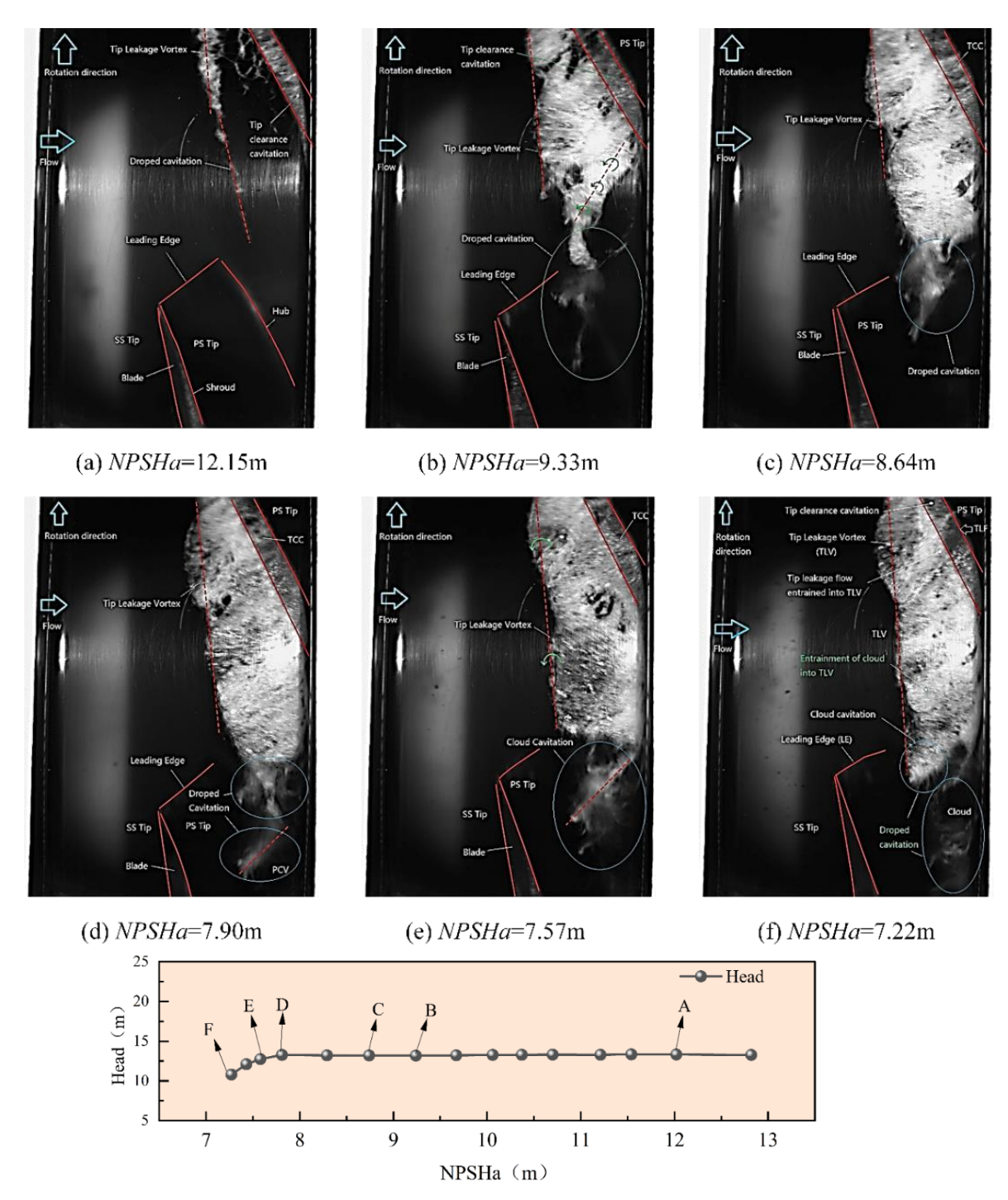


Fig. 10 Cavitation flow structure and its evolution law at different NPSHa

cavitation triangle, with the downstream cavitation undergoes collapse as it approaches the blade's pressure surface.

As the impeller rotates to 48° , the detached cloud cavitation at the blade tip moves toward the neighboring blade in the tip region, contributing to flow separation near the pressure surface and causing a marked decline in pump performance. At 60° of rotation, cloud cavitation on the blade's pressure surface undergoes complete collapse, driven by the combined effects of tip leakage flow and turbulence within the blade-to-blade flow. The detached cloud cavitation reorients perpendicularly to the pressure surface, giving rise to a Perpendicular Cavitation Vortex.

3.8 Cavitation Flow Structure and Its Evolution Law of Different Devices Under *Npsha* Conditions

To provide a clearer visualization of how cavitation flow structures vary under different NPSH conditions, Fig. 10 presents the internal cavitation flow structures of the jet pump impeller at the same rotational position (36°) for various NPSH values along the cavitation performance curve. At NPSH = 12.15 m, the pump head remains stable. Numerous detached vortex filaments appear at the leading edge of the blades. The tip-leakage vortex cavitation begins to detach early and collapses near the mid-passage. At NPSH = 9.33 m, the pump head exhibits noticeable fluctuations. The blade tip becomes fully covered with

vapor bubbles, and a triangular cavitation region starts to form. Large vapor bubbles begin to shed from the tail of the cloud cavitation and migrate toward the adjacent blade's pressure surface. Some bubbles migrate toward the pressure side of the blade, while others move toward the tip clearance. Bubbles moving toward the pressure side obstruct the flow passage, leading to flow separation. Their collapse on the pressure surface also contributes to surface erosion and material damage. At NPSH = 8.64 m, the pump head is affected, indicating a transitional stage of cavitation development. Vapor bubbles at the blade tip become increasingly dense, and the triangular cavitation region extends further downstream, covering a larger portion of the blade tip. Large-scale detached cloud cavitation migrate closer to the pressure surface. At NPSH = 7.90 m, cavitation reaches the I critical condition. Large vapor bubbles shed from the tail of the cloud cavitation and move toward adjacent blades. Some bubbles move toward the pressure side, obstructing the flow and inducing flow separation. Their collapse contributes to erosion on the blade surface. Others enter the tip clearance and are entrained by the tip leakage flow from adjacent blades, and reorient nearly perpendicular to nearly perpendicular to the pressure surface, forming distinct vertical cavitation vortices. At NPSH = 7.57 m, the blade tip triangular cavitation region extends downstream along the main flow direction along the main flow. Entrainment by tip leakage flow and agitation by the mainstream lead to the formation of large, rolling vapor bubbles at the blade tip. The detached cloud cavitation begins to reorient perpendicularly and migrate closer to the pressure surface. Overall, cavitation fully envelops the blade tip region, and the pump head corresponds to a 3% drop in pump head on the performance curve. This condition is defined as critical cavitation. At NPSH = 7.22m, cavitation fills the tip clearance and directly enters the tip leakage vortex, and is transported downstream under the suction effect of the vortex. Simultaneously, cloud cavitation begins to shed from the end of the triangular cavitation region. The detached vapor clouds rupture and collapse as they move downstream and toward the pressure surface. A a significant decline in pump head is observed on the performance curve, indicating cavitation breakdown. As the pressure decreases and sheet cavitation progressively covers the suction surface of the blades, inter-vortex interference occurs in the overlapping regions of two adjacent blades. The vertical cavitation vortex extends from the suction surface of the initiating blade to the pressure surface of the neighboring blade. As the vertical cavitation vortex stretches between blades, cavitation breakdown occurs, effectively obstructing the upper region of the rotor passage. This vortex structure is primarily associated with tip clearance leakage. The leakage flow alters the velocity distribution near the blade tip, generating a velocity gradient corresponding to the pressure-side cavitation vortex (PCV), which in turn induces a vorticity distribution oriented along the vortex axis.

As shown in Fig. 11, the vapor volume fraction in the impeller region is quantified via binarization of cavitation images. Quantitative measurements confirm

that the cavitation area ratio grows monotonically from 2.737% at stage A to 10.678% at B, 15.883% at C, 16.455% at D, 28.518% at E, and 30.019% at F. This increasing trend indicates that, as NPSH is reduced and pump head correspondingly drops, a larger fraction of the blade passage becomes occupied by vapor. Notably, the relatively small increase from C to D (15.883% to 16.455%) suggests a modest expansion of the cavitation pocket of the cavitation pocket, whereas the large jump from D to E signals the onset of critical cavitation. This sharp expansion coincides with crossing the NPSH3 threshold (the 3% head loss criterion), implying that pump head will undergo substantial degradation beyond this point. As the cavitation region extends to nearly one-third of the passage in stages E and F, its interference with the flow becomes highly disruptive. The enlarged cavity likely blocks a significant portion of the suction flow, inducing flow separation and significantly increasing blade drag. This blockage and separation explain the pronounced performance deterioration observed at very low NPSHa.

4. CONCLUSION

This study presents a comprehensive experimental investigation into cavitation flow structures in a water-jet pump, with particular focus on the dynamic evolution of cavitation under varying operating conditions. It addresses a critical gap in the literature—namely, the absence of detailed flow visualizations that directly correlate specific cavitation modes with pump performance degradation. By employing high-speed imaging, the study establishes a clear connection between internal flow behavior and the onset of cavitation-induced performance losses. The major findings are quantitatively presented and supported by performance curves, image binarization, and vapor volume analysis. The observed phenomena are thoroughly interpreted through the lens of vortex dynamics and internal flow instabilities, and these interpretations are well supported by experimental data, ensuring that all conclusions are solidly based on experimental evidence. To visualize the cavitation zones and vortex structures during cavitation development, high-speed visualizations of cavitating flows across various NPSH conditions are provided and summarizes the following key conclusions:

- 1. The cavitation patterns observed in the pump under varying NPSHa conditions include Sheet Cavitation, Cloud Cavitation, Tip Clearance Cavitation, Tip Leakage Vortex Cavitation, and Perpendicular Cavitation Vortex.
- 2. High-speed visualizations under various cavitation conditions were used to analyze the cavitation vortex structures in the water-jet pump, revealing distinct spatial distributions and development paths for each type.
- 3. Analysis of cavitation performance curves and flow field evolution shows that, as cavitation intensifies, vortex structures—particularly Perpendicular Cavitation Vortices (PCVs)—expand and interact across adjacent blade passages, resulting in flow blockage, separation, and a sharp decline in head and efficiency during the breakdown stage.

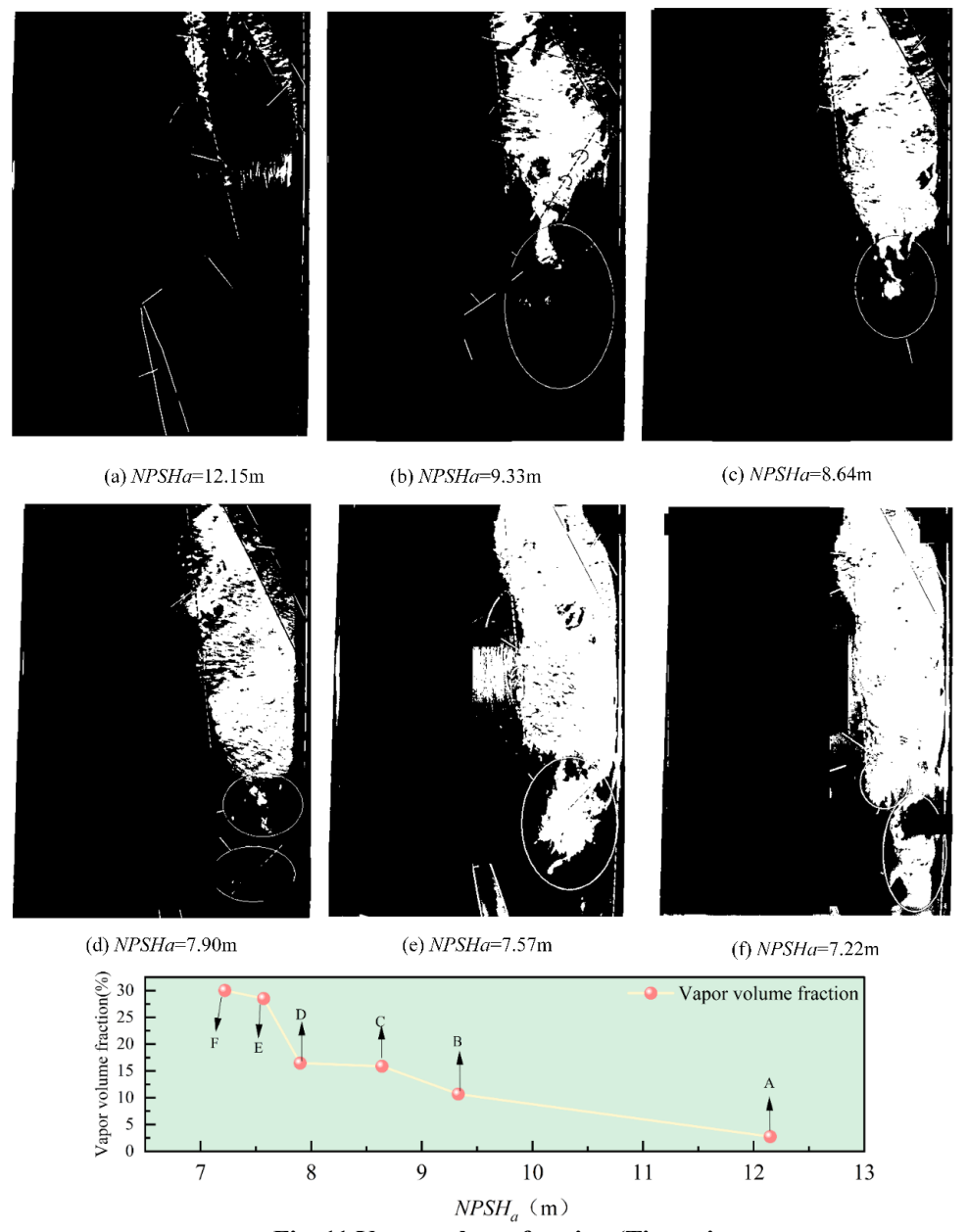


Fig. 11 Vapor volume fraction (Tip region

- 4. The study provides a detailed characterization of the development and evolution mechanisms of sheet cavitation, cloud cavitation, tip clearance cavitation, tip leakage vortex cavitation, and vertical cavitation vortices. It is observed that vertical cavitation vortices extending between neighboring blades can block flow passages. Furthermore, it is confirmed that tip leakage vortex cavitation intensifies under severe cavitation conditions.
- 5. The study proposes practical engineering strategies to mitigate cavitation effects. These include optimizing blade-tip geometry and guide-vane design to suppress destructive vortex formation, as well as adjusting operational parameters to delay cavitation onset, thereby improving pump performance and reliability.

FUNDING

This work was funded by the China Postdoctoral Science Foundation Funded Project (2023M733355,

Grant No.2019M651734), Jiangsu University Youth Talent Development Program (2020), the Chunhui Program Cooperative Scientific Research Project of the Ministry of Education, Research Project of State Key Laboratory of Mechanical System and Vibration (MSV202203), Natural Science Foundation of China (Grant No.51906085, Grant U20A20292). This work also Supported by the Open Project Program of Shandong Marine Aerospace Equipment Technological Innovation Center, Ludong University (Grant No. MAETIC202211)

CONFLICT OF INTEREST

The author declares that there are no financial or non-financial conflicts of interest to disclose.

AUTHORS' CONTRIBUTIONS

Long Yun: Funding Acquisition, Methodology. Tian Chenbiao: Data Curation, Writing, Review &

Editing, Visualization. **Zhu Rongsheng:** Formal Analysis, Supervision. **Wang Dezhong:** Conceptualization, Methodology, Supervision. **Chen Jianping:** Investigation, Methodolog, Validation. All authors: Writing – Review & Editing, Approval of the final manuscript.

REFERENCES

- Dehghan, A. A., & Shojaeefard, M. H. (2022). Experimental and numerical optimization of a centrifugal pump volute and its effect on head and hydraulic efficiency at the best efficiency point. Proceedings of the Institution of Mechanical Engineers, Part C: Journal of Mechanical Engineering Science, 236(9), 4577–4598. https://doi.org/10.1177/09544062211056019
- Dehghan, A. A., Shojaeefard, M. H., & Roshanaei, M. (2024). Exploring a new criterion to determine the onset of cavitation in centrifugal pumps from an energy-saving standpoint; experimental and numerical investigation. *Energy*, 293, 130681. https://doi.org/10.1016/j.energy.2024.130681
- Franc, J. -P., & Michel, J. -M. (2006). Fundamentals of cavitation (Vol. 76). Dordrecht, The Netherlands: Springer Science & Business Media. https://doi.org/10.1007/1-4020-2233-6
- Laberteaux, K. R., Ceccio, S. L., Mastrocola, V. J., & Lowrance, J. L. (1998). High speed digital imaging of cavitating vortices. *Experiments in Fluids*, 24(5–6), 489–498. https://doi.org/10.1007/s003480050198
- Li, D., Fu, X., Zuo, Z., Wang, H., Li, Z., Liu, S., & Wei, X. (2019). Investigation methods for analysis of transient phenomena concerning design and operation of hydraulic-machine systems—A review. *Renewable and Sustainable Energy Reviews*, 101, 26–46. https://doi.org/10.1016/j.rser.2018.10.023
- Liu, H. L., Liu, D. X., Wang, Y., Du, H., & Xu, H. (2011). Numerical research status and prospects of cavitating flow in a pump. *Fluid Machinery*, *39*(9), 38–44. https://doi.org/10.3969/j.issn.1005-0329.2011.09.009
- Long, Y., An, C., Zhu, R., & Chen, J. (2021). Research on hydrodynamics of high velocity regions in a waterjet pump based on experimental and numerical calculations at different cavitation conditions. *Physics of Fluids*, 33(4), 045124. https://doi.org/10.1063/5.0040618
- Luo, X.-W., Ji, B., & Tsujimoto, Y. (2016). A review of cavitation in hydraulic machinery. *Journal of Hydrodynamics*, 28(3), 335–358. https://doi.org/10.1016/S1001-6058(16)60638-8
- Pan, Z., & Yuan, S. (2013). Fundamentals of cavitation in pumps [in Chinese]. Zhenjiang, China: Jiangsu University Press.
- Pearsall, I. S. (1957). The use of high-speed photography in the study of cavitation. *The Journal of*

- *Photographic Science*, *5*(5), 105–111. https://doi.org/10.1080/00223638.1957.11736604
- Pearsall, I. S. (1974). Cavitation. *The Chartered Mechanical Engineer*, 21(7), 79–85.
- Rains, D. A. (1954). Tip clearance flows in axial flow compressors and pumps (Ph.D. dissertation). California Institute of Technology, Pasadena, CA, USA. https://doi.org/10.7907/MR84-WZ87
- Shao, C., Gu, B., & Chen, Y. (2010). Measurement of steady and unsteady flow in centrifugal pump spiral casing using PIV. *Transactions of the Chinese Society of Agricultural Engineering*, 26(7), 128–133. https://doi.org/10.3969/j.issn.1002-6819.2010.07.023
- Shi, L. (2016). Research on tip leakage vortex structure and cavitation mechanism in three-dimensional hydrofoil and axial flow pump (Doctoral dissertation). Jiangsu University, Zhenjiang, China.
- Tan, D., Li, Y., Wilkes, I., Vagnoni, E., Miorini, R. L., & Katz, J. (2015). Experimental investigation of the role of large scale cavitating vortical structures in performance breakdown of an axial waterjet pump. *Journal of Fluids Engineering*, 137(11), 111301. https://doi.org/10.1115/1.4030614
- Tong, Z., Liu, H., Cao, X. E., Westerdahl, D., & Jin, X. (2023). Cavitation diagnosis for water distribution pumps: An early-stage approach combining vibration signal-based neural network with high-speed photography. Sustainable Energy Technologies and Assessments, 55, 102919. https://doi.org/10.1016/j.seta.2022.102919
- Westra, R. W., Broersma, L., van Andel, K., & Kruyt, N. P. (2010). PIV measurements and CFD computations of secondary flow in a centrifugal pump impeller. *Journal of Fluids Engineering*, *132*(6), 061104. https://doi.org/10.1115/1.4001803
- Willard, G. W. (1953). Ultrasonically induced cavitation in water: A step-by-step process. *The Journal of the Acoustical Society of America*, 25(4), 669–686. https://doi.org/10.1121/1.1907161
- Wu, Y., Liu, S., Yuan, H., & Shao, J. (2011). PIV measurement on internal instantaneous flows of a centrifugal pump. *Science China Technological Sciences*, 54, 270–276. https://doi.org/10.1007/s11431-010-4262-3
- Zhang, N., Liu, X., Gao, B., Wang, X., & Xia, B. (2019). Effects of modifying the blade trailing edge profile on unsteady pressure pulsations and flow structures in a centrifugal pump. *International Journal of Heat and Fluid Flow*, 75, 227–238. https://doi.org/10.1016/j.ijheatfluidflow.2019.01.00
- Zhao, X., Shen, X., Geng, L., Zhang, D., & van Esch, B. B. (2022). Effects of cavitation on the hydrodynamic loading and wake vortex evolution of a pre-swirl pump-jet propulsor. *Ocean Engineering*, 266,

Y. Long et al. / *JAFM*, Vol. 19, No. 1, pp. 3429-3443, 2026.

113069.

https://doi.org/10.1016/j.oceaneng.2022.113069